Conductivities of Titan's dusty ionosphere

O. Shebanits[1], J-E. Wahlund[1], J. H. Waite Jr[2]. and M. K. Dougherty[3]

[1]Swedish Institute of Space Physics, Uppsala, Sweden

[2]Southwest Research Institute, San Antonio, USA

[3]Imperial College London, London, UK

Corresponding author: Oleg Shebanits (oleg.shebanits@irfu.se)

Key Points:

- Second peak of Pedersen conductivity in dusty plasma region of Titan's ionosphere
- Indications of reverse Hall effect near ~900 km altitude
- Up to x10 difference between dayside and nightside conductivities

Abstract

Titan's ionosphere hosts a globally distributed non-trivial dusty ion-ion plasma, providing an environment for studies of dusty ionospheres that is in many aspects unique in our solar system. Thanks to the Cassini mission, Titan's ionosphere also features one of the largest dusty plasma datasets from 126 flybys of the moon over 13 years, from 2004 to 2017.

Recent studies have shown that negatively charged dust dramatically alters the electric properties of plasmas, in particular planetary ionospheres. Utilizing the full plasma content of the moon's ionosphere (electrons, positive ions and negative ions/dust grains), we derive the electric conductivities and define the conductive dynamo region.

Our results show that using the full plasma content increases the Pedersen conductivities at ~1300 km altitude by 20% compared to the earlier estimates without charged dust, while the Hall conductivities indicate a reverse Hall effect at ~900 km altitude (closest approach) and below. The dayside conductivities are shown to be factor ~7-9 larger than on the nightside, owing to higher dayside plasma densities.

Plain Language Summary

The largest moon of Saturn, Titan, is famous for its signature orange haze that is formed in the top layer of its atmosphere – ionosphere. The complex organic chemistry initiated mainly by sunlight forms grains of dust that at ~1000 km altitude reach a few nanometers in size (comparable to finely ground flour). These grains of dust become charged in the ionosphere by absorbing the free electrons (depleting them). Below ~1000 km altitude there are almost no electrons left. In the absence of light electrons (negative charge), the positively charged ions instead become the dominant mobile charge carrier, as the negatively charged dust is much heavier. Such a reversal of charge mobility has a large impact on the electric properties of an ionosphere, increasing its electric conductivity and changing the direction of its electric currents.

We use a dataset from the Cassini mission spanning an entire solar cycle and nearly half a Titan year (≈15 Earth years) to calculate the electric conductivities of Titan's ionosphere and show that the dusty plasma increases them by 20% on average. Below 1000 km altitudes, we find

indications of a secondary conductive layer, a direct consequence of the dust grains absorbing the electrons.

1 Introduction

Titan is immersed in Saturn's magnetosphere (Bertucci et al., 2008; Garnier et al., 2010) and does not have its own magnetic field. Instead, an induced magnetic field is formed around Titan from the interactions with Saturn's magnetosphere, similarly to interactions of Venus and Mars with the solar wind and interplanetary magnetic field (e.g., Bertucci et al., 2011 and references therein). The interaction between Titan and the ambient magnetic field depends to a large degree on Titan's conductive ionosphere. Previously, the electrical properties of Titan's ionosphere were derived using only the ion and electron content (Rosenqvist et al., 2009). However, in the later years, significant amounts of charged dust were detected in Titan's ionosphere (Ågren et al., 2012; Coates et al., 2007; Shebanits et al., 2013) and a globally present dusty ion-ion plasma is expected (Shebanits et al., 2016). The charged dust grains in the ionosphere-like plasma of Enceladus plume (Morooka et al., 2011) and in the near-equatorial dusty ionosphere of Saturn (Morooka et al., 2019) were shown to have a profound effect on its electric conductivities by Simon et al. (2011) and Yaroshenko & Lühr (2016), and Shebanits et al. (2020), respectively. In this work we derive the electrical properties of Titan's ionosphere using the full plasma content: electrons, positive ions and negative ions/dust grains. The relevant in-situ measurements used here are from the Radio and Plasma Wave Science Langmuir Probe (RPWS/LP, Gurnett et al., 2004), the Ion and Neutral Mass Spectrometer (INMS, Teolis et al., 2015; Waite et al., 2004) and the Cassini Fluxgate Magnetometer (MAG, Dougherty et al., 2004). The dataset spans the entire Cassini mission and is representative of a full solar cycle and nearly half Titan year.

2 Observations and Method

2.1 Datasets and flyby coverage

We use data from 58 flybys where measurements of the Cassini INMS, RPWS/LP and the Cassini MAG are simultaneously available (**T#:** A, B, 5, 16-21, 23, 25-30, 32, 34, 36, 38-40, 42-44, 46, 48-51, 55-59, 61, 65, 71, 77, 83, 84, 86, 87, 91, 92, 95, 98, 100, 104, 107, 108, 113, 116-121). The Cassini RPWS/LP dataset provides electron temperatures (Ågren et al., 2009) and electron densities, positive ion densities, negative ion densities, derived as described in Shebanits et al. (2016). The primary data from the INMS are the neutral densities (CH_4 and N_2). The INMS ion data is used as supplementary for the ion mass information in the RPWS/LP analysis (Shebanits et al., 2016).

Magnetic field data from Cassini MAG: magnetic field strength.

2.2 Method

Conductivities

Using the conductivity tensor representation (Schunk & Nagy, 2009) with dust term added (Shebanits et al., 2020; Simon et al., 2011; Yaroshenko & Lühr, 2016), the Pedersen (σ_P), Hall (σ_H) and magneticl field parallel ($\sigma_\parallel$) conductivities are defined as:

$$\sigma_P = \sum_{s=e,i,d} n_s \frac{q_s}{B} \frac{\nu_s \Omega_s}{\nu_s^2 + \Omega_s^2}$$
$$\sigma_H = -\sum_{s=e,i,d} n_s \frac{q_s}{B} \frac{\Omega_s^2}{\nu_s^2 + \Omega_s^2} \quad (1)$$
$$\sigma_\parallel = \sum_{s=e,i,d} \frac{n_s q_s^2}{m_s \nu_s}$$

Here the subscripts (s) denotes electrons (e), positive ions (i) and negative ions/dust grains (d) and the input plasma parameters are number density (n), mass (m), charge (q), momentum transfer collision frequency (ν), gyrofrequency (Ω) and magnetic field strength (B).
Strictly speaking, the equations for conductivities must be summed over all the plasma species. However, mass spectra information is of very limited availability for Titan's ionosphere. We therefore adopt the average masses for the positive ions and for the negative ions/dust grains as described in Shebanits et al. (2016). Additionally, singly-charged negative ions/dust grains are assumed. This approach is validated using a test case of T40 flyby where the mass spectra for the positive ions and the negative ions and dust grains are available simultaneously (Coates et al., 2009; Shebanits et al., 2016), see Appendix A.

Momentum Transfer Collision frequencies

In the following equations, the number density is always in cm^{-3}, the rest of the units are SI. It should be noted that since the RPWS/LP measures the total charged particle flux at a given bias voltage and the availability of the mass spectra is limited, we use the total charge densities for the positive ions and negative ions/dust grains together with their respective mean mass as derived and validated in Shebanits et al. (2016). The collision frequencies (and in turn, conductivities) therefore represent mass-averages as well.
The momentum transfer collision frequencies (MTCFs) are largely dominated by collisions with neutrals. However, in a dusty plasma a significant contribution from collisions with the negative ions/dust grains is present and cannot be discarded (Shebanits et al., 2020; Yaroshenko & Lühr, 2016). We therefore use the total MTCF for each species as a sum of collision frequencies with the other species:

$$\nu_{s,tot} = \sum_{t \neq s} \nu_{st}$$

The main neutral species in Titan's atmosphere are N_2 and CH_4 (Niemann et al., 2005; Waite et al., 2005). Collisions of electrons with N_2 and CH_4 are implemented as hard-sphere collisions (e.g., Schunk & Nagy, 2009) with the appropriate electron-dependent cross-sections $\chi(T_e)$ for N_2 (Itikawa, 2006) and CH_4 (Song et al., 2015):

$$\nu_{e-neutral} = n_{neutral} \frac{8}{3} \sqrt{\frac{2k_b T_e}{\pi m_e}} \chi_{neutral}(T_e) \quad (2)$$

For the negative ion/dust collisions with neutrals, both elastic (Coulomb) and hard-sphere collisions are used (see also Shebanits et al., 2020). For the hard-sphere collisions, the cross-sections are replaced by the average dust grain cross-section πR_d^2, where the average dust grain

radius R_d is estimated from the average grain mass by assuming a spherical grain and a mass density of kerogen (1280 ± 300 kgm^{-3}, Stankiewicz et al., 2015):

$$\nu_{d-neutral} = \frac{8}{3\sqrt{\pi}} \frac{n_n m_n}{m_d + m_n} \sqrt{2k_b \frac{m_n T_d + m_d T_n}{m_n m_d}} \pi R_d^2 \quad (3)$$

It should be noted that the actual dust grain geometry in Titan's ionosphere is likely to be of fractal nature (e.g. Chatain et al., 2020; Michael et al., 2011; Shebanits et al., 2016; Sittler et al., 2009; Waite et al., 2009). However, extensive lab experiments and sophisticated modelling are required to produce a database of dust grain geometries (and their cross-sections) at Titan. We therefore adapt spherical grains as a first order approximation.

Elastic collisions of electrons and neutrals with the heavy charged species are calculated according to Schunk & Nagy (2009), their eq. 4.144 & eq. 4.88, respectively:

$$\nu_{e-i,d} = 54.5 \frac{n_{i,d} Z_{i,d}^2}{T_e^{1.5}}, \quad (4)$$

$$\nu_{i,d-neutral} = 2.5879 \times 10^{-9} n_n \sqrt{\frac{Y_n}{m_{i,d}} \frac{m_n}{m_n + m_{i,d}}}, \quad (5)$$

where the charge number is defined as $Z_{i,d} = q_{i,d}/|q_e|$.
MTCF equation for elastic collisions between the positive ions and negative ions/dust grains (ion-dust drag) is the same as ion-ion collision (eq. 4.142 in Schunk & Nagy, 2009):

$$\nu_{id} = 1.27\, Z_d^2 Z_i^2 \frac{n_d}{m_i} (m_i + m_d) \sqrt{\frac{m_d m_i}{(m_i T_d + m_d T_i)^3}} \quad (6)$$

3 Results and Discussion

3.1 Dynamo region

The MTCFs and gyrofrequencies defining the conductive dynamo region of Titan's ionosphere are shown in Figure 1, plotted in altitude with the solar zenith angle (SZA) colorcoded. The error bars are symmetric and represent the combined measurement uncertainty (2σ level). The statistical means of the dynamo region boundaries from all included flybys are given in solid black lines, with standard deviations as dashed lines.
The top boundary of the positive ions is at 1390 ± 90 km, in agreement with previous estimates (Rosenqvist et al., 2009). The negative ions and dust grains begin to conduct at ~100 km higher altitudes due to their higher mass and subsequently lower gyrofrequency (see also Shebanits et al., 2020). However, since the negative ions and dust grains are nearly absent above 1200 km altitude in Titan's ionosphere, their impact on the top boundary of the dynamo region is negligible.

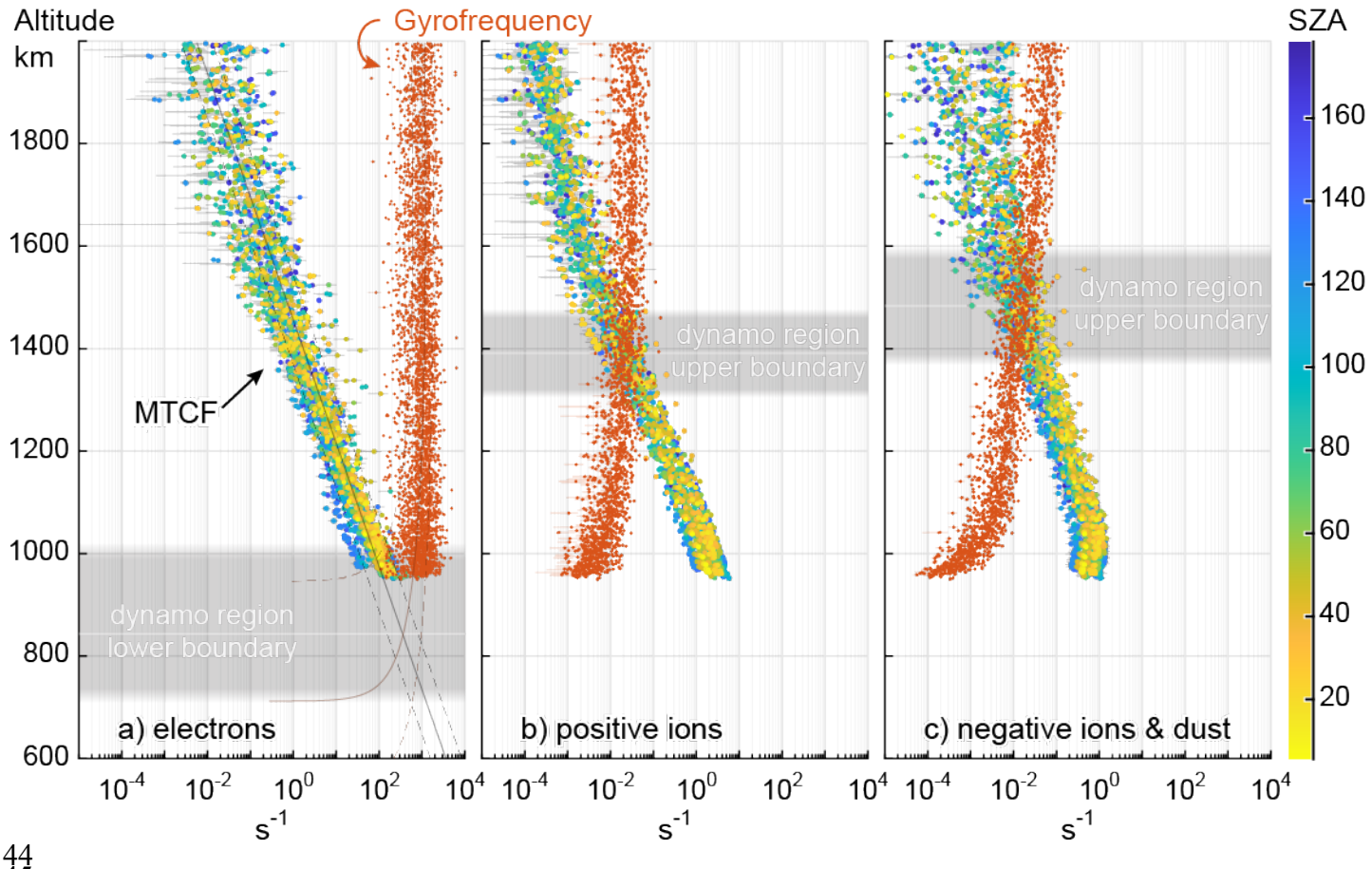

*Figure 1. Momentum transfer collision frequencies (color-coded by SZA) and gyrofrequencies (orange) for electrons (panel **a**), positive ions (panel **b**) and negative ions/dust grains (panel **c**). The dynamo region boundary statistics from all included flybys: the mean values are shown as solid black lines and the corresponding standard deviations as dashed lines. For the lower boundary, the electron frequencies are extrapolated as defined in the text.*

It should be noted that the lower boundary defined by electrons (panel a) is a rough estimate derived from an exponential extrapolation of the electron MTCFs and a linear extrapolation of their gyrofrequencies. Given the absence of magnetic field measurements below the closest approach, a more sophisticated extrapolation is not deemed necessary for this work. In light of this, the lower boundary is constrained to be between 700 and 1000 km altitude, with lower altitudes more likely in the nightside ionosphere as indicated by the SZA trend (blue end of the colorbar = nightside). Incidentally, the dusty plasma in Titan's ionosphere is expected to peak below 1000 km (Shebanits et al., 2016). More on this below.

The rather large variability in the top dynamo region boundary (Figure 1) is a combination of the variabilities in the background neutral densities, magnetic field, SZA and arguably also the local time. This is illustrated in Figure 2, where the top boundaries for positive ions are plotted in the leftside panels a1 & a2 and for negative ions and dust grains in the rightside panels b1 & b2 (throughout the text, the panels in figures are labeled with letters for columns and numbers for rows, for easier referencing). The magnetic field strength $|B|$ is proportional to marker size and the local time is colorcoded. Solid black lines are moving medians (50-points window).

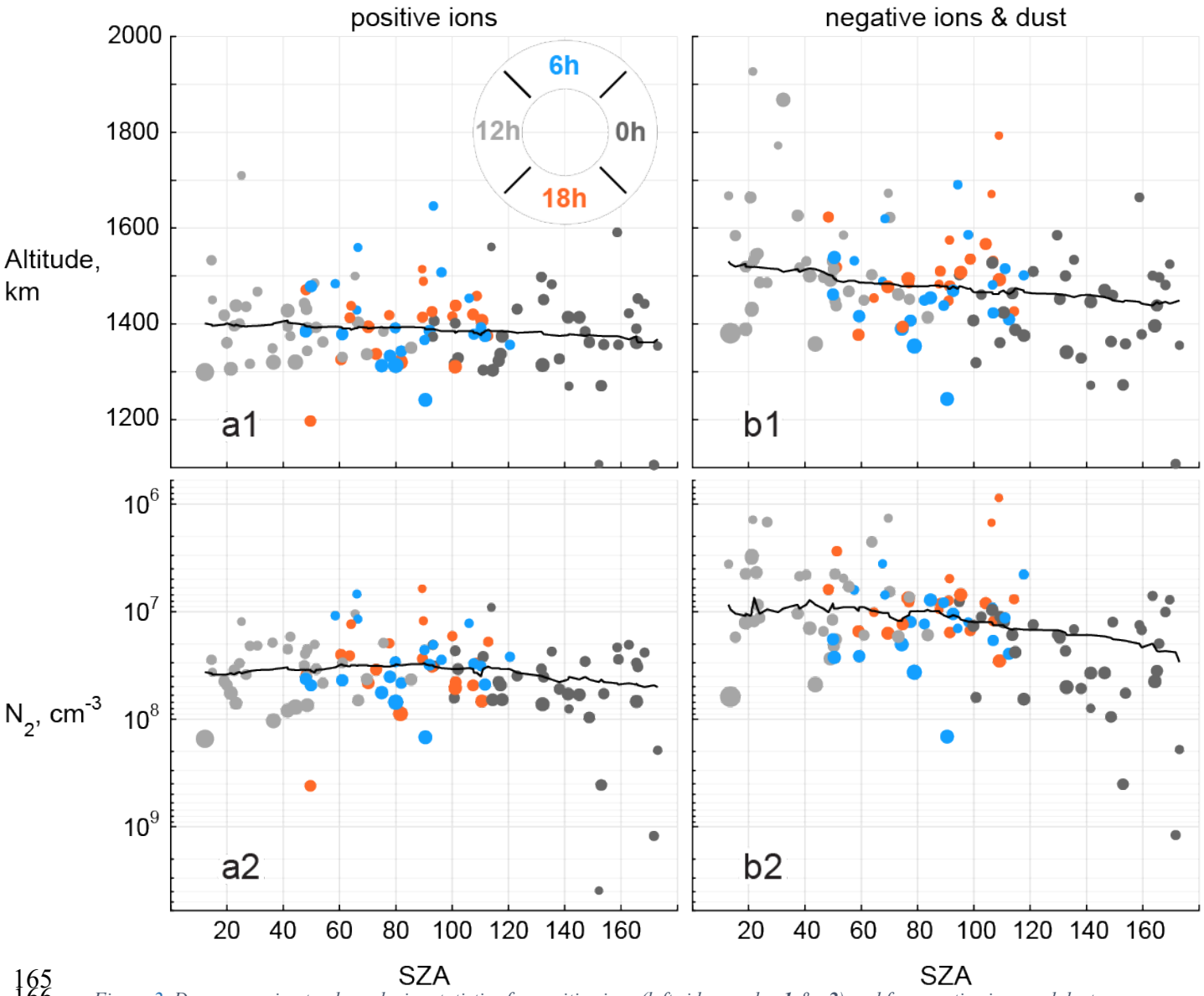

*Figure 2. Dynamo region top boundaries statistics for positive ions (left side panels **a1** & **a2**) and for negative ions and dust grains (right side panels **b1** & **b2**), plotted in altitude (top panels **a1** & **b1**) and in the measured N_2 densites (bottom panels **a2** & **b2**) versus SZA. Size of markers is proportional to the magnetic field strength $|B|$. Titan Local Time is color-coded.*

The most obvious factor is $|B|$, with stronger field (larger markers) corresponding to lower altitudes (panels a1, b1) and higher neutral densities (panels a2, b2). The SZA dependency is noticeable for the negative ions and dust grains but is much weaker for the positive ions, propagated from their respective masses. Although for the negative ions the median is roughly linearly decreasing in altitude from dayside to nightside (panel b1), when plotted in the background neutral densities instead (panel b2) the decrease is only clear on the nightside, likely due to cooling and contraction of the neutral atmosphere. There seems to be a slight difference between dawn (blue) and dusk (orange) regions for the negative ions and dust grains (right side, panels b1 & b2), but with the current dataset it is statistically not conclusive.

3.2 Conductivities

Titan's ionospheric conductivities are shown in Figure 3 versus altitude (left side, panels a1-3) and measured N_2 densities (right side, panels b1-3), color-coded with SZA. The error bars are symmetric and represent the combined uncertainties of measurements, collision cross-sections and masses of heavy plasma species (2σ level). The error bars are one-sided for points where the uncertainties reach zero (omitted on log scale to reduce clutter). The square markers in panels a2 and b2 mark negative values of σ_H. The empty markers in all panels show the data points with low signal to noise ratio (positive ion densities $< 10\ cm^{-3}$). The field parallel conductivities $\sigma_\parallel$ separating into two profiles above ~1400 km altitude clearly demonstrate this, with the left profile (lower values) essentially showing the measurement limit of $\sigma_\parallel$ for that region.

The SZA trends for the ionospheric conductivities are inherited from the ionospheric plasma number densities, with σ_P and σ_H being roughly linearly proportional to the positive ion densities and $\sigma_\parallel$ to the electron densities.

Pedersen conductivities σ_P have a peak between 1200 and 1400 km altitude and increase sharply below 1100 km. At altitudes of ~1400 km, $\sigma_H > \sigma_P$ and the Hall currents are the dominant horizontal currents (Ågren et al., 2011). However, at the CA the σ_H drops due to the increasing presence of the dusty plasma. In a dusty plasma, σ_H is expected to reverse (reverse Hall effect) due to the electron depletion onto the dusty grains (Muralikrishna & Kulkarni, 2006; Shebanits et al., 2020; Simon et al., 2011; Yaroshenko & Lühr, 2016). The small cluster of data points marked with a circle in panels a2 & b2 is indicative of this reversal (square markers are $\sigma_H < 0$). With σ_H quenched or reversed and σ_P increasing below the CA, it is therefore possible that a secondary layer of Pedersen current exists when the bottom boundary of the dynamo region extends enough to include the dusty plasma region below 900 km altitude.

Comparing the altitude profiles (panels a1-3) to the profiles versus measured neutral densities (panels b1-3), the latter are more structured. Evidently, some of the variability below 1100 km altitudes can be attributed to the variability of the neutral atmosphere. In particular, the increase of the Pedersen conductivity below 1100 km altitude is clearer, with the nightside values at 1000 km altitude corresponding to 5×10^9 cm^{-3}, again consistent with Titan's atmosphere contracting on the nightside.

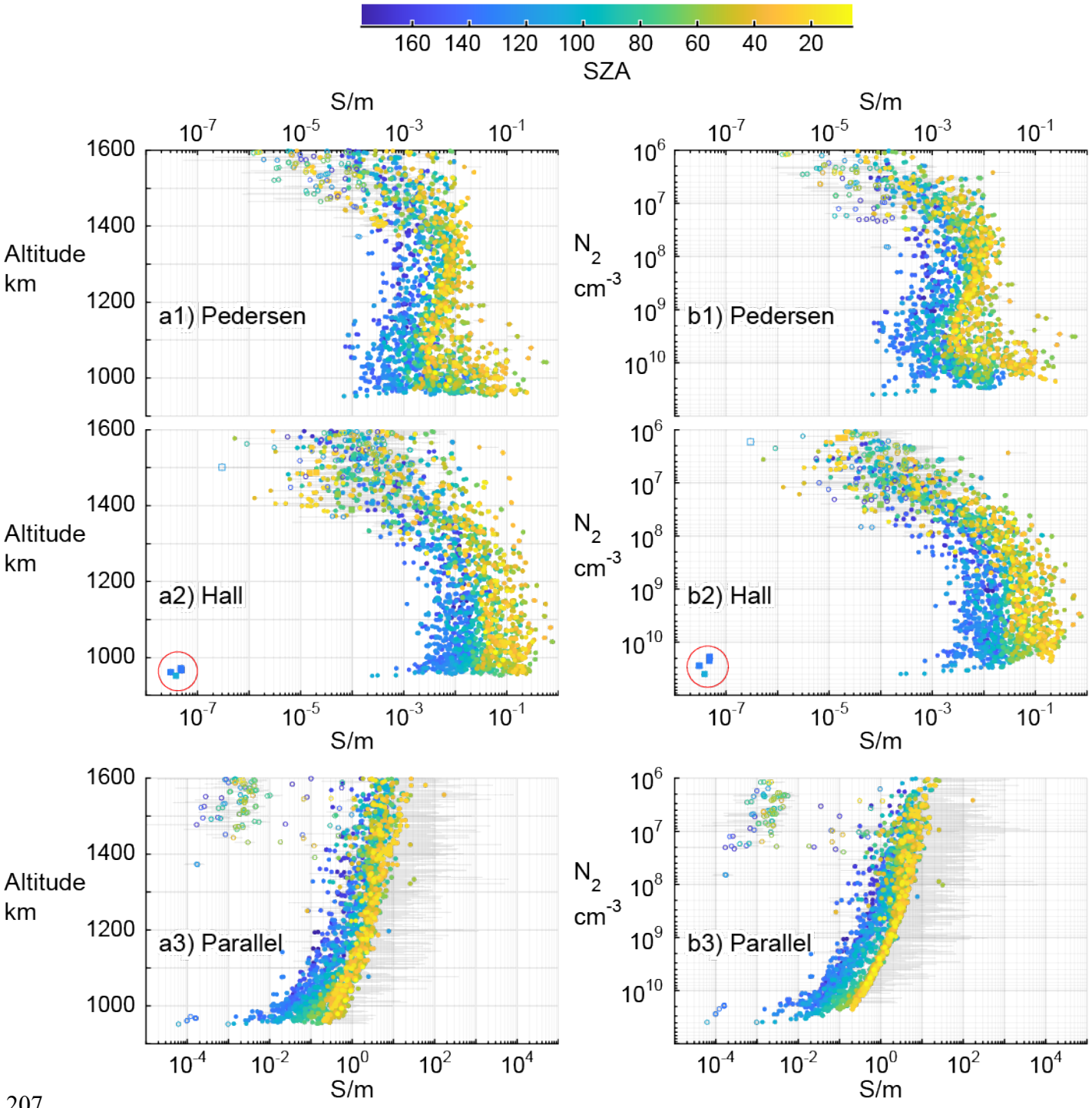

*Figure 3. Titan's ionospheric conductivities: Pedersen (panels **a1**, **b1**), Hall (**a2**, **b2**) and Parallel (**a3**, **b3**), plotted in altitude (left-side panels **a1-3**) and the measured N_2 densities (right-side panels **b1-3**). The SZA is color-coded. Red circle marks negative Hall conudctivities (reverse Hall effect).*

3.3 Dusty plasma influence

The sharp increase in σ_P near closest approach (CA) was also evident in the earlier study and attributed to the decrease of the magnetic field strength (Rosenqvist et al., 2009), pre-dating the

discovery of the negative ions/dust grains in the RPWS data (Ågren et al., 2012; Shebanits et al., 2013).

Interestingly, although the increase of σ_P does coincide with an increase in positive ion and negative ion/dust densities, the main influence is indeed the decrease in the magnetic field. This is evident in Figure 4 which shows σ_P (left panels a1 & a2) and σ_H (right panels b1 & b2) below 1200 km altitude plotted versus magnetic field strength $|B|$. On the nightside the impact of $|B|$ is much weaker for both σ_P and σ_H. It is worth mentioning that the trend in $|B|$ persists regardless of the nominal corotational plasma ram direction.

As mentioned above, the presence of dusty plasma strongly diminishes or even reverses σ_H. In Titan's ionosphere, a low electron depletion ratio n_e/n_i (colorcoded) has been demonstrated to be a sufficient indicator for a dusty plasma (Shebanits et al., 2016). In Figure 4, the electron depletion ratio is colorcoded (dark = dusty) and the n_e/n_i trend in σ_H is clearly visible for the nightside ionosphere (panel b2) and to some extent also on the dayside (panel b1). This is in agreement with a globally present dusty plasma in Titan's ionosphere (Shebanits et al., 2016) and introduces a layer of complexity to the ionospheric current system that is unique to Titan so far.

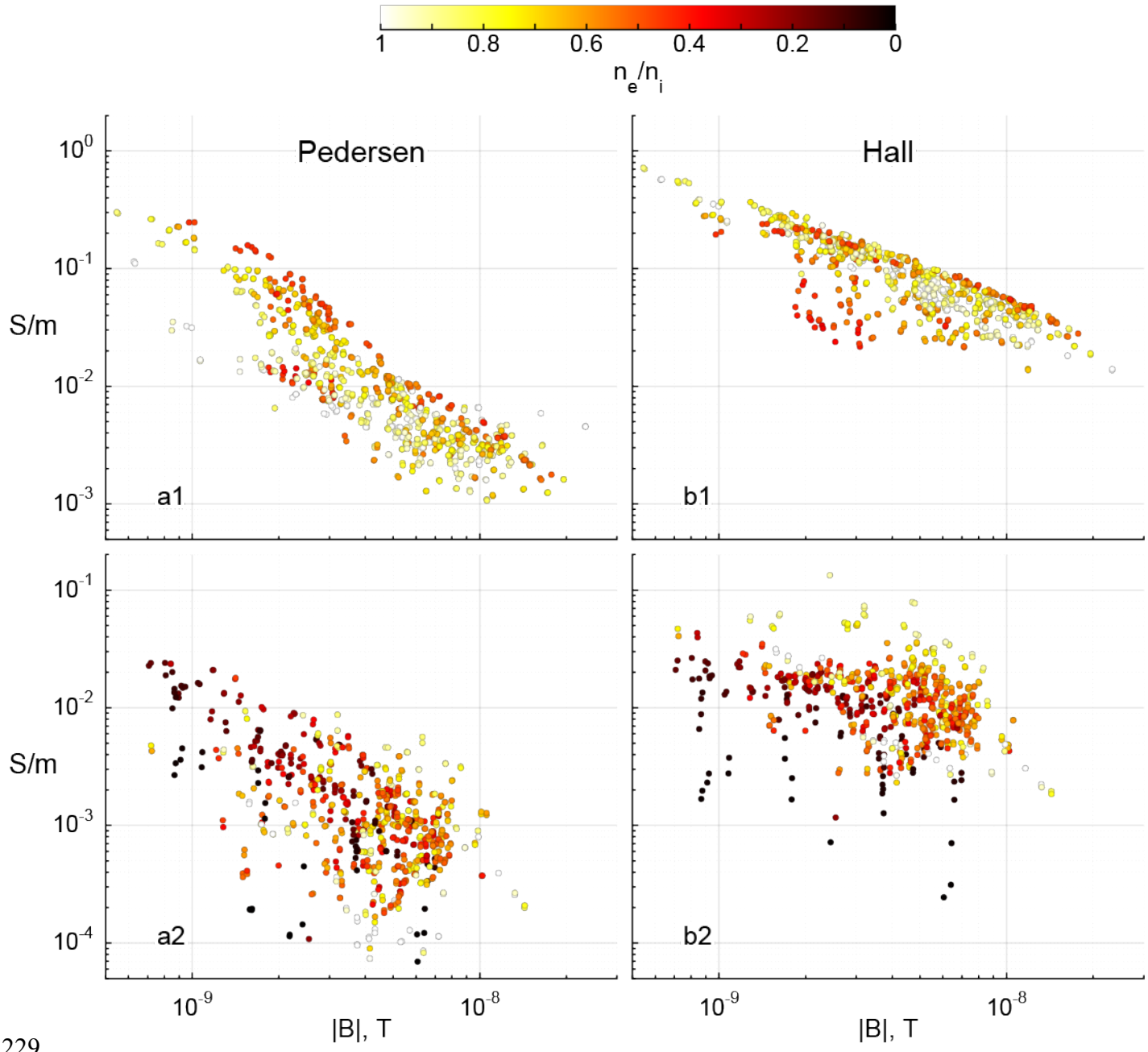

*Figure 4. Pedersen (left panels **a1** & **a2**) and Hall (right panels **b1** & **b2**) conductivities **below 1200 km** plotted versus magnetic field strength |B|. The electron depletion ratio n_e/n_i (color-coded) indicates the regions of dusty plasma. Top panels **a1** & **b1** show dayside ionosphere (SZA < 90°), bottom panels **a2** & **b2** show nightside (SZA > 90°).*

3.4 General picture

Median profiles of the conductivities from Figure 3 are shown in Figure 5 versus the measured N_2 densities (panels a1-3) and versus altitude (panels b1-3), colorcoded into dayside ($SZA < 70$, orange), terminator ($70 \leq SZA < 100$, green) and nightside ($SZA \geq 100$, blue) regions. Notably, σ_P peaks plotted in altitude (panel b1) appear broader on the dayside and terminator than on the nightside. This is an effect of the neutral atmosphere shifting in altitude between day and night, as evident when plotting versus the measured neutral densities instead (panel a1). As

mentioned above, the differences in the dayside, terminator and nightside profiles follow the respective positive ion density profiles (electrons for field-parallel conductivity), with the upper peak altitude increasing towards the terminator and roughly stabilizing towards the nightside (Ågren et al., 2009; Shebanits et al., 2017).

The total median profiles are shown in black. Panels c1-3 show the total median profiles without charged dust (Rosenqvist et al., 2009) in red (marked R2009), to be compared with the medians from current work: solid black line for all flybys and dashed red line for the 17 flybys included in R2009. Comparing the total median profile to the R2009, it is evident that including the dusty plasma shifts the first σ_P peak down in altitude by ~100 km. Expanding the dataset with the later flybys increases this peak by ~20%. This increase is consistent with the enhancement of plasma densities during the solar maximum between 2011 and 2015 (Edberg et al., 2013; Shebanits et al., 2017). The profiles in panels a1-3 & b1-3 are therefore medians over a full solar cycle and nearly half a Titan year.

The deviations between the R2009 profile and this work are attributed to two major differences. Firstly, in the current work we treat the full plasma content – including the charged dust grains – whereas Rosenqvist et al. (2009) predated the dust detection in the RPWS/LP data. Secondly, we use the neutral densities measured in-situ by the INMS, while Rosenqvist et al. (2009) relied on an atmospheric model by Müller-Wodarg et al. (2008) – this is why the $\sigma_{\parallel}$ medians differ so much above 1200 km in panel c3. However, despite this, the total median profiles for the 17 flybys from R2009 are in a remarkable agreement down to ~1000 km with deviations only appearing near the CA. This again demonstrates that in Titan's ionosphere at altitudes above ~1000 the σ_H and σ_P are mainly governed by the positive ions.

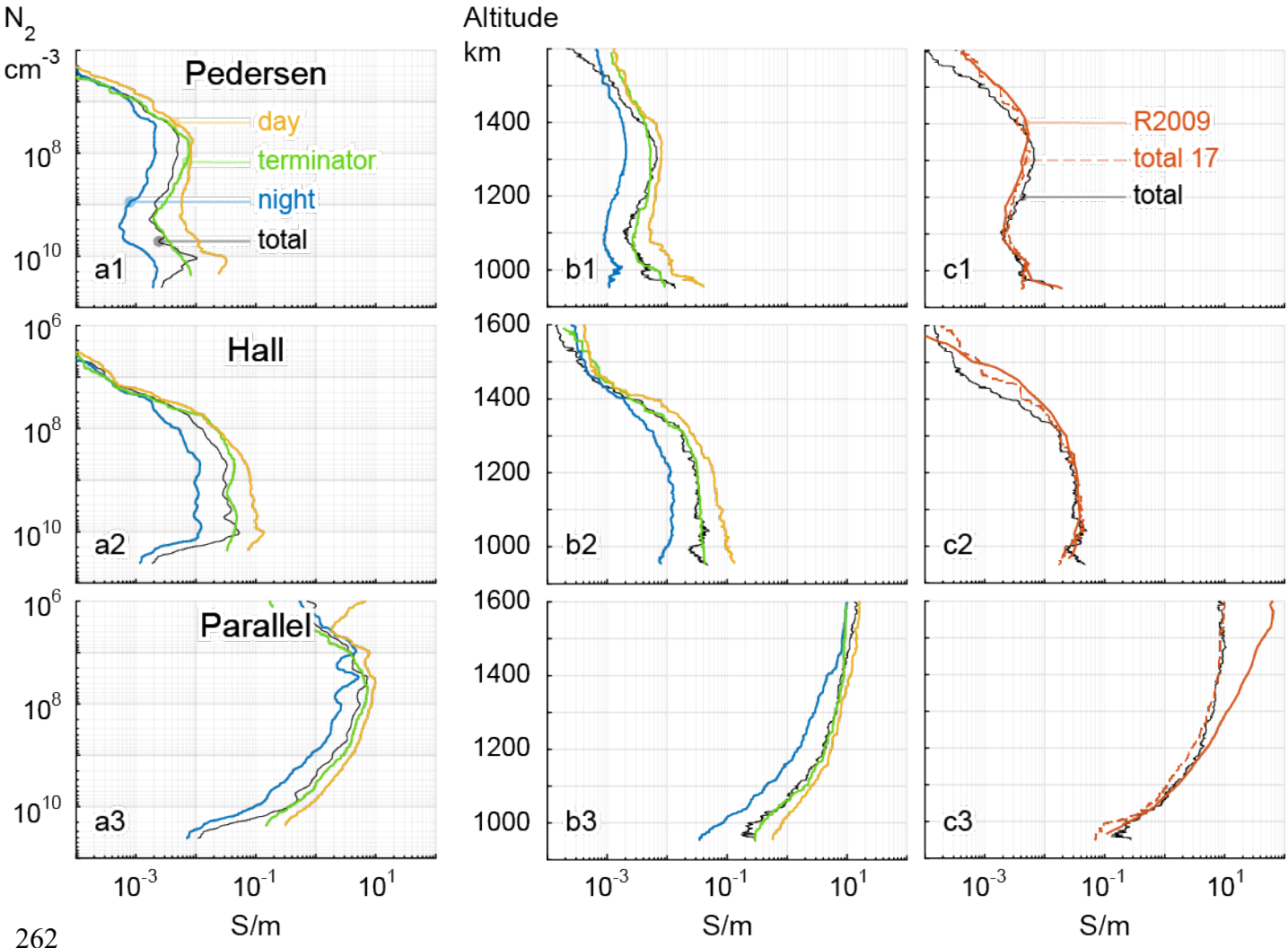

*Figure 5. General conductivity profiles for all included flybys: Pedersen (panels **a1**, **b1** & **c1**), Hall (panels **a2**, **b2** & **c2**) and Parallel (panels **a3**, **b3** & **c3**). Panels **a1-3** show sliding quadratic regressions with 400 point window (over N_2 densities). The rest of the panels show sliding medians with a 200-point window (over altitudes). The total medians are in solid black. The panels **c1-3** also show the medians of the 17 flybys included in the Rosenqvist et al. (2009), with the R2009 profile as a solid red line and the same flybys from current work as a dashed red line. The colored lines are medians for the dayside ($SZA < 70$, yellow), terminator ($70 \leq SZA < 100$, green) and nightside ($SZA \geq 100$, blue).*

Comparing Titan's dusty ionosphere with that of Saturn, the impact of charged dust on the conductivities is very different. On Saturn, the Pedersen conductivities were increased by up to two orders of magnitude and the Hall conductivities reduced or reversed already above the upper peak of ionospheric plasma densities (Shebanits et al., 2020). On Titan, although a 20% increase in corresponding upper peak of Pedersen conductivities is evident, the real impact becomes prominent near the CA. This is because the sources of the dust grains are different. On Saturn, the dust grains fall in from the D-ring (Hamil et al., 2018; e.g., Hsu et al., 2018; Mitchell et al., 2018) in addition to possibly forming in the top ionosphere (Waite et al., 2018), and are already present in significant quantities in the top ionosphere (Morooka et al., 2019), well above the main photoionization peak (Hadid et al., 2018). On Titan, the dust grains are chemically formed in the ionosphere itself (Desai et al., 2017; Lavvas et al., 2013; Vuitton et al., 2009; Waite et al.,

2007) and reach densities comparable to electrons and positive ions well below the photoionization peak.

4 Conclusions

- The Pedersen and Hall conductivities in Titan's ionosphere down to ~1000 km altitudes are governed mainly by the positive ions.
- Dusty plasma influence on the Pedersen conductivity is measurable at ~1300 km altitude but most impact is below ~1000 km altitude (also for the Hall conductivity).
- The magnetic field strength remains the main factor for the increase in Pedersen conductivity at ~900-1100 km altitudes.
- The bulk of Titan's ionosphere in the 1000-1400 km altitude range is dominated by the Hall conductivity. Subsequently, Hall currents are expected to be the dominant horizontal currents.
- The sharp increase of the Pedersen conductivity below 1100 km altitude coincides with the dusty region of Titan's ionosphere, suggesting a dusty plasma layer dominated by the Pedersen conductivity (and subsequently, Pedersen currents).
- The Hall conductivity shows indications of a reverse Hall effect at ~950 km altitude.

Acknowledgments

O.S. acknowledges funding by SNSA Dnr 195/20. J.-E.W. acknowledges the support of the Cassini RPWS/LP operations by SNSA. J.H.W. worked under internal funding from the Division of Space Science and Engineering, Southwest Research Institute. M.K.D. acknowledges funding by Royal Society Research Professorship RP140004.

Datasets availability: the dataset used in the current study is available in a Mendeley Data repository, doi: 10.17632/hwc5wfbvj9.1.

Appendix A

A validation of using the total densities and average masses of the heavy plasma species is performed for the case of T40 (Figure 6a), where the mass spectra are available simultaneously for the positive ions (Shebanits et al., 2016) and negative ions/dust grains (Coates et al., 2009). The solid lines represent the average Pedersen (blue), Hall (red) and magnetic field parallel (yellow) conductivity profiles, all in a very good agreement with the respective conductivities derived using the full mass spectra (square markers). The corresponding plasma charge densities are shown for reference (panel b).

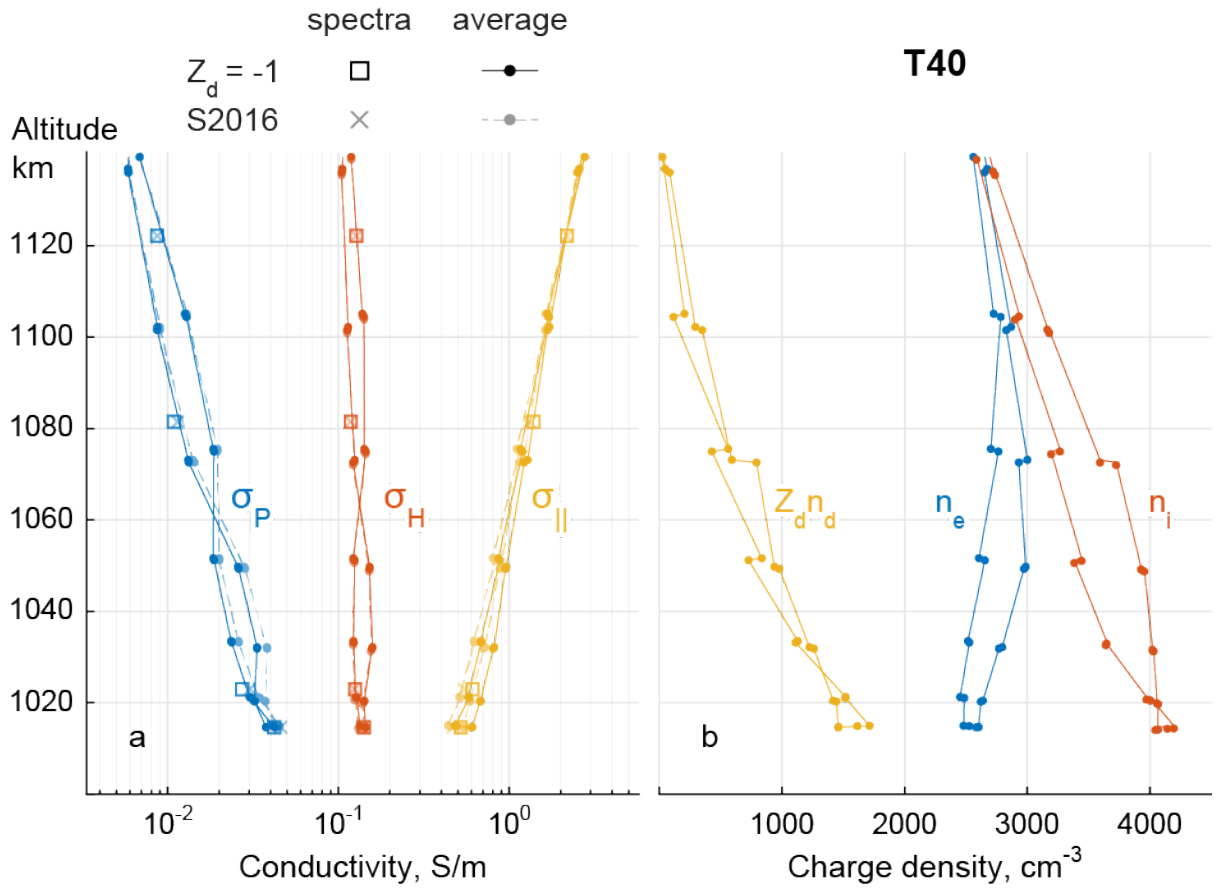

*Figure 6. Panel **a**: Comparison of the T40 conductivities derived using the average plasma species masses (solid lines with circle markers) and using the full mass spectra (squares and crosses) of the positive ions and negative ions/dust. Squares and solid lines are derived assuming singly charged particles, fainter crosses and dashed lines are derived using the empirical negative ion and dust grain charge estimate (Shebanits et al., 2016). Panel **b**: the plasma densities are shown for reference.*

One of the parameters associated with the size and shape of the grains is the charge. Empirical estimate of the average dust grain charge suggests values between -1.5 and -2.5 for flybys T16, T29, T40 and T56 (Shebanits et al., 2016), while theoretical predictions (for spherical grains) suggest most likely charge to be $Z_d = -1$ (Draine & Sutin, 1987; Meyer-Vernet, 2013). The impact of the grain charge can be seen in Figure 6a, where the singly charged grains are used for the solid lines and the empirically estimated Z_d is used for the dashed lines and. The difference between these cases is <5% and is approximately a third of the combined measurement uncertainties. For this reason, the conductivities for all flybys are derived assuming $Z_d = -1$.

References

Ågren, K., Wahlund, J.-E., Garnier, P., Modolo, R., Cui, J., Galand, M., & Müller-Wodarg, I. (2009). On the ionospheric structure of Titan. *Planetary and Space Science*, *57*(14–15), 1821–1827. https://doi.org/10.1016/j.pss.2009.04.012

Ågren, K., Andrews, D. J., Buchert, S. C., Coates, A. J., Cowley, S. W. H., Dougherty, M. K., et al. (2011). Detection of currents and associated electric fields in Titan's ionosphere from Cassini data. *Journal of Geophysical Research: Space Physics*, *116*(4), A04313.

https://doi.org/10.1029/2010JA016100

Ågren, K., Edberg, N. J. T., & Wahlund, J. E. (2012). Detection of negative ions in the deep ionosphere of Titan during the Cassini T70 flyby. *Geophysical Research Letters*, *39*(10), n/a-n/a. https://doi.org/10.1029/2012GL051714

Bertucci, C., Achilleos, N., Dougherty, M. K., Modolo, R., Coates, A. J., Szego, K., et al. (2008). The magnetic memory of Titan's ionized atmosphere. *Science*, *321*(5895), 1475–1478. https://doi.org/10.1126/science.1159780

Bertucci, C., Duru, F., Edberg, N., Fraenz, M., Martinecz, C., Szego, K., & Vaisberg, O. (2011). The Induced Magnetospheres of Mars, Venus, and Titan. *Space Science Reviews*, *162*(1–4), 113–171. https://doi.org/10.1007/s11214-011-9845-1

Chatain, A., Carrasco, N., Ruscassier, N., Gautier, T., Vettier, L., & Guaitella, O. (2020). Interaction dust – plasma in Titan's ionosphere: An experimental simulation of aerosols erosion. *Icarus*, *345*(March), 113741. https://doi.org/10.1016/j.icarus.2020.113741

Coates, A. J., Crary, F. J., Lewis, G. R., Young, D. T., Waite, J. H., Sittler, E. C., & Sittler, J. C. (2007). Discovery of heavy negative ions in Titan's ionosphere. *Geophysical Research Letters*, *34*(22), L22103. https://doi.org/10.1029/2007GL030978

Coates, A. J., Wellbrock, A., Lewis, G. R., Jones, G. H., Young, D. T., Crary, F. J., & Waite, J. H. (2009). Heavy negative ions in Titan's ionosphere: Altitude and latitude dependence. *Planetary and Space Science*, *57*(14–15), 1866–1871. https://doi.org/DOI 10.1016/j.pss.2009.05.009

Desai, R. T., Coates, A. J., Wellbrock, A., Vuitton, V., Crary, F. J., González-Caniulef, D., et al. (2017). Carbon Chain Anions and the Growth of Complex Organic Molecules in Titan's Ionosphere. *The Astrophysical Journal*, *844*(2), L18. https://doi.org/10.3847/2041-8213/aa7851

Dougherty, M. K., Kellock, S., Southwood, D. J., Balogh, A., Smith, E. J., Tsurutani, B. T., et al. (2004). The Cassini Magnetic Field Investigation. *Space Science Reviews*, *114*(1–4), 331–383. https://doi.org/10.1007/s11214-004-1432-2

Draine, B. T., & Sutin, B. (1987). Collisional charging of interstellar grains. *The Astrophysical Journal*, *320*, 803. https://doi.org/10.1086/165596

Edberg, N. J. T., Andrews, D. J., Shebanits, O., Ågren, K., Wahlund, J. E., Opgenoorth, H. J., et al. (2013). Solar cycle modulation of Titan's ionosphere. *Journal of Geophysical Research: Space Physics*, *118*(8), 5255–5264. https://doi.org/10.1002/jgra.50463

Garnier, P., Dandouras, I., Toublanc, D., Roelof, E. C., Brandt, P. C., Mitchell, D. G., et al. (2010). Statistical analysis of the energetic ion and ENA data for the Titan environment. *Planetary and Space Science*, *58*(14–15), 1811–1822. https://doi.org/10.1016/j.pss.2010.08.009

Gurnett, D. A., Kurth, W. S., Kirchner, D. L., Hospodarsky, G. B., Averkamp, T. F., Zarka, P., et al. (2004). The Cassini radio and plasma wave investigation. *Space Science Reviews*, *114*(1–4), 395–463. https://doi.org/DOI 10.1007/s11214-004-1434-0

Hadid, L. Z., Morooka, M. W., Wahlund, J. -E., Persoon, A. M., Andrews, D. J., Shebanits, O., et al. (2018). Saturn's Ionosphere: Electron Density Altitude Profiles and D-Ring Interaction From The Cassini Grand Finale. *Geophysical Research Letters*, *46*(16), 9362–9369. https://doi.org/10.1029/2018GL078004

Hamil, O., Cravens, T. E., Reedy, N. L., & Sakai, S. (2018). Fate of Ice Grains in Saturn's Ionosphere. *Journal of Geophysical Research: Space Physics*, *123*(2), 1429–1440. https://doi.org/10.1002/2017JA024616

Hsu, H.-W., Schmidt, J., Kempf, S., Postberg, F., Moragas-Klostermeyer, G., Seiß, M., et al. (2018). In situ collection of dust grains falling from Saturn's rings into its atmosphere. *Science*, *362*(6410), eaat3185. https://doi.org/10.1126/science.aat3185

Itikawa, Y. (2006). Cross Sections for Electron Collisions with Nitrogen Molecules. *Journal of Physical and Chemical Reference Data*, *35*(1), 31–53. https://doi.org/10.1063/1.1937426

Lavvas, P., Yelle, R. V., Koskinen, T., Bazin, A., Vuitton, V., Vigren, E., et al. (2013). Aerosol growth in Titan's ionosphere. *Proceedings of the National Academy of Sciences*, *110*(8), 2729–2734. https://doi.org/10.1073/pnas.1217059110

Meyer-Vernet, N. (2013). On the charge of nanograins in cold environments and Enceladus dust. *Icarus*, *226*(1), 583–590. https://doi.org/10.1016/j.icarus.2013.06.014

Michael, M., Tripathi, S. N., Arya, P., Coates, A., Wellbrock, A., & Young, D. T. (2011). High-altitude charged aerosols in the atmosphere of Titan. *Planetary and Space Science*, *59*(9), 880–885. https://doi.org/10.1016/j.pss.2011.03.010

Mitchell, D. G., Perry, M. E., Hamilton, D. C., Westlake, J. H., Kollmann, P., Smith, H. T., et al. (2018). Dust grains fall from Saturn's D-ring into its equatorial upper atmosphere. *Science*, *362*(6410), eaat2236. https://doi.org/10.1126/science.aat2236

Morooka, M. W., Wahlund, J. E., Eriksson, A. I., Farrell, W. M., Gurnett, D. A., Kurth, W. S., et al. (2011). Dusty plasma in the vicinity of Enceladus. *Journal of Geophysical Research-Space Physics*, *116*(A12). https://doi.org/Doi 10.1029/2011ja017038

Morooka, M. W., Wahlund, J.-E. J. -E. E., Hadid, L. Z., Eriksson, A. I., Edberg, N. J. T. T., Vigren, E., et al. (2019). Saturn's Dusty Ionosphere. *Journal of Geophysical Research: Space Physics*, *124*(3), 1679–1697. https://doi.org/10.1029/2018JA026154

Müller-Wodarg, I. C. F., Yelle, R. V., Cui, J., & Waite, J. H. (2008). Horizontal structures and dynamics of Titan's thermosphere. *Journal of Geophysical Research*, *113*(E10), E10005. https://doi.org/10.1029/2007JE003033

Muralikrishna, P., & Kulkarni, V. H. (2006). On the height variation of the E-region cowling

conductivity – effect of charged dust particles. *Annales Geophysicae*, *24*(11), 2949–2957. https://doi.org/10.5194/angeo-24-2949-2006

Niemann, H. B., Atreya, S. K., Bauer, S. J., Carignan, G. R., Demick, J. E., Frost, R. L., et al. (2005). The abundances of constituents of Titan's atmosphere from the GCMS instrument on the Huygens probe. *Nature*, *438*(7069), 779–784. https://doi.org/10.1038/nature04122

Rosenqvist, L., Wahlund, J. E., Ågren, K., Modolo, R., Opgenoorth, H. J., Strobel, D., et al. (2009). Titan ionospheric conductivities from Cassini measurements. *Planetary and Space Science*, *57*(14–15), 1828–1833. https://doi.org/10.1016/j.pss.2009.01.007

Schunk, R., & Nagy, A. (2009). *Ionospheres* (2nd ed.). Cambridge: Cambridge University Press. https://doi.org/10.1017/CBO9780511635342

Shebanits, O., Wahlund, J. E., Mandt, K., Ågren, K., Edberg, N. J. T., & Waite, J. H. (2013). Negative ion densities in the ionosphere of Titan-Cassini RPWS/LP results. *Planetary and Space Science*, *84*, 153–162. https://doi.org/10.1016/j.pss.2013.05.021

Shebanits, O., Wahlund, J.-E., Edberg, N. J. T., Crary, F. J., Wellbrock, A., Andrews, D. J., et al. (2016). Ion and aerosol precursor densities in Titan's ionosphere: A multi-instrument case study. *Journal of Geophysical Research: Space Physics*, *121*(10), 10,075-10,090. https://doi.org/10.1002/2016JA022980

Shebanits, O., Vigren, E., Wahlund, J. -E., Holmberg, M. K. G., Morooka, M., Edberg, N. J. T., et al. (2017). Titan's ionosphere: A survey of solar EUV influences. *Journal of Geophysical Research: Space Physics*, *122*(7), 7491–7503. https://doi.org/10.1002/2017JA023987

Shebanits, O., Hadid, L. Z., Cao, H., Morooka, M. W., Hunt, G. J., Dougherty, M. K., et al. (2020). Saturn's near-equatorial ionospheric conductivities from in situ measurements. *Scientific Reports 2020 10:1*, *10*(1), 1–13. https://doi.org/10.1038/s41598-020-64787-7

Simon, S., Saur, J., Kriegel, H., Neubauer, F. M., Motschmann, U., & Dougherty, M. K. (2011). Influence of negatively charged plume grains and hemisphere coupling currents on the structure of Enceladus' Alfvén wings: Analytical modeling of Cassini magnetometer observations. *Journal of Geophysical Research: Space Physics*, *116*(A4), n/a-n/a. https://doi.org/10.1029/2010JA016338

Sittler, E. C., Ali, A., Cooper, J. F., Hartle, R. E., Johnson, R. E., Coates, A. J., & Young, D. T. (2009). Heavy ion formation in Titan's ionosphere: Magnetospheric introduction of free oxygen and a source of Titan's aerosols? *Planetary and Space Science*, *57*(13), 1547–1557. https://doi.org/10.1016/j.pss.2009.07.017

Song, M.-Y., Yoon, J.-S., Cho, H., Itikawa, Y., Karwasz, G. P., Kokoouline, V., et al. (2015). Cross Sections for Electron Collisions with Methane. *Journal of Physical and Chemical Reference Data*, *44*(2), 023101. https://doi.org/10.1063/1.4918630

Stankiewicz, A., Ionkina, N., Motherwell, B., Bennett, B., Wint, O., & Mastalerz, M. (2015). Kerogen Density Revisited—Lessons From the Duvernay Shale. In *Proceedings of the 3rd*

Unconventional Resources Technology Conference. Tulsa, OK, USA: American Association of Petroleum Geologists. https://doi.org/10.15530/urtec-2015-2157904

Teolis, B. D., Niemann, H. B., Waite, J. H., Gell, D. A., Perryman, R. S., Kasprzak, W. T., et al. (2015). A Revised Sensitivity Model for Cassini INMS: Results at Titan. *Space Science Reviews*, *190*(1–4), 47–84. https://doi.org/10.1007/s11214-014-0133-8

Vuitton, V., Lavvas, P., Yelle, R. V., Galand, M., Wellbrock, A., Lewis, G. R., et al. (2009). Negative ion chemistry in Titan's upper atmosphere. *Planetary and Space Science*, *57*(13), 1558–1572. https://doi.org/10.1016/j.pss.2009.04.004

Waite, J. H., Lewis, W. S., Kasprzak, W. T., Anicich, V. G., Block, B. P., Cravens, T. E., et al. (2004). The Cassini Ion and Neutral Mass Spectrometer (INMS) investigation. *Space Science Reviews*, *114*(1–4), 113–231. https://doi.org/10.1007/s11214-004-1408-2

Waite, J. H., Niemann, H., Yelle, R. V., Kasprzak, W. T., Cravens, T. E., Luhmann, J. G., et al. (2005). Ion Neutral Mass Spectrometer results from the first flyby of Titan. *Science*, *308*(5724), 982–986. https://doi.org/10.1126/science.1110652

Waite, J. H., Young, D. T., Cravens, T. E., Coates, A. J., Crary, F. J., Magee, B., & Westlake, J. (2007). The Process of Tholin Formation in Titan's Upper Atmosphere. *Science*, *316*(5826), 870–875. https://doi.org/10.1126/science.1139727

Waite, J. H., Young, D. T., Westlake, J. H., Lunine, J. I., McKay, C. P., & Lewis, W. S. (2009). High-Altitude Production of Titan's Aerosols. In *Titan from Cassini-Huygens* (pp. 201–214). Dordrecht: Springer Netherlands. https://doi.org/10.1007/978-1-4020-9215-2_8

Waite, J. H., Perryman, R. S., Perry, M. E., Miller, K. E., Bell, J., Cravens, T. E., et al. (2018). Chemical interactions between Saturn's atmosphere and its rings. *Science*, *362*(6410), eaat2382. https://doi.org/10.1126/science.aat2382

Yaroshenko, V. V., & Lühr, H. (2016). Electrical conductivity of the dusty plasma in the Enceladus plume. *Icarus*, *278*, 79–87. https://doi.org/10.1016/j.icarus.2016.05.033

References in supporting information must also be included in the reference list of the main paper, or in a designated section in the main paper, so that they will be discovered, linked, and indexed. A separate list in the supporting information is not necessary. References are not included in word counts for excess length fees. Data sets that are not newly reported as part of this research should also be cited in the references. New data sets or software that are deposited elsewhere with a permanent identifier should be cited. AGU follows the Joint Declaration of Data Citations Principles.

All references must be available to readers at the time of publication; there should be no "unpublished", in preparation, under review, or "in press" references. Please write the respective journal with any questions.

An example of a reference:

Deng, A., & Stauffer, D. R. (2006), On improving 4-km mesoscale model simulations. *Journal of Applied Meteorology and Climatology*, *45*(3), 361–381. doi:10.1175/JAM2341.1

More information on reference formatting with examples can be found in our Brief Guide to AGU Style.

Figure 1. The figure caption should begin with an overall descriptive statement of the figure followed by additional text. They should be immediately after each figure. Figure parts are indicated with lower-case letters (**a, b, c…**). For initial submission, please place both the figures and captions in the text near where they are cited rather than at the end of the file (not both). At revision, captions can be placed in-text or at the end of the file, and figures should be uploaded separately. Each figure should be one complete, cohesive file (please do not upload sub-figures or figure parts in separate files).

Table 1. Start this caption with a short description of your table. Format tables using the Word Table commands and structures. Additional information on table formatting can be found in our Style Guide, Table Formatting. Do not create tables using spaces or tabs characters. Large tables presenting rich data should be presented as separate excel or .csv files, not as part of the main text.